PLY INTERFACE ANGLES TO PROMOTE AUTOMATED FORMING OF AEROSPACE STRUCTURES

K. J. Johnson[1], A. T. Rhead[2], E. G. Loukaides[3] and R. Butler[4]

MAST Research Centre, Department of Mechanical Engineering, University of Bath, Claverton Down, Bath, BA2 7AY, UK

Email: [1]K.J.Johnson@bath.ac.uk, [2]A.T.Rhead@bath.ac.uk, [3]E.Loukaides@bath.ac.uk [4]R.Butler@bath.ac.uk,

Keywords: Automation, Defects, Fibre Angle, Formability, Stacking Sequence

ABSTRACT

The success of an automated vacuum forming process where flat prepreg laminates are formed into parts with complex curvature, is heavily influenced by the capacity of plies to deform during the forming procedure. Understanding the deformation behaviour in single and multi-layer prepreg arrangements gives insight into the likelihood of defect generation and the possible solutions which lead to defect free parts. The paper presents a theoretical model based on eigenvector and eigenvalue analysis to determine compatible modes of deformation within individual ply interfaces and complete stacking sequences. The model is validated using an experimental process where laminates are formed onto a doubly curved tool geometry using an industrial double diaphragm former. Stacking sequences with 90° interface angles outline the most formable solutions, whereas continuous 45° interfaces that spiral e.g. 45/0/-45/90 outline the most problematic forming conditions due to a locking behaviour. Optimising the interface angle within a stack for maximum compatibility is shown to completely remove defects at elevated temperature. Interface angles and stacking sequence are thus seen to be as significant as temperature and vacuum rate on the quality of formed parts.

1 INTRODUCTION

The reduction in manufacturing cost of structural composite parts within the aerospace sector has been established as a key area for advancement, if increased use of composite materials is to be feasible. Formability presents a vital aspect within the process of manufacturing composite components. This is particularly essential for the widely implemented automated manufacturing techniques, which improve rate of production. The associated risk however, is the generation of defects during the process of multi-layer forming. A common defect that can arise from plies being restricted from inter-ply and intra-ply shearing, is for laminates to produce out-of-plane wrinkles [1]. These wrinkles can cause severe performance knock downs and therefore need to be avoided during the manufacturing process [2]. In order to prevent the generation of wrinkles during automated vacuum forming processes such as Hot Drape forming (HDF) or Double Diaphragm forming (DDF), it becomes necessary to investigate which parameters could trigger or minimise the chances of wrinkles appearing.

Previously, three factors have been investigated which influence the process of vacuum forming laminates. The first being temperature, the higher the temperature, the lower the resin viscosity and thus the easier it is to form the laminates into curvature [3]. The second parameter is the tool geometry. Tools with complex double curvature require much higher shear strain in the laminate, making ease of forming a function of tool geometry. Pressure presents the third forming parameter. The pressure involved in vacuum forming operations generally encompasses full atmospheric pressure. The slower the application of pressure, the more time is available for fibres to shift and slip

between each other. An approach to artificially increase the ply mobility has been to position veil materials in between plies, which mimic the effect of decreased resin viscosity while being able to perform the forming operating at a lower temperature [4]. Recently there has been one more forming parameter indicated; laminate stacking sequence. Initial studies carried out by Hallander [5] suggest that stacking sequence has an influence and can potentially be the cause of defect generation or defect avoidance. However, there have not been any attempts to outline how exactly the ply interaction within a stacking sequence could result in a more or less formable laminate.

The aim of this paper is to outline the importance of interface angle in ply stacking sequences, on forming behavior of laminates. By establishing a theoretical foundation for ply deformation, both in single and multi-layer arrangements, analytical prediction can be provided on the ease of forming with regards to any given stacking sequence. The presented theory is supported by experimental work, where laminates are formed over a doubly curved tool geometry using an automated forming procedure.

2 EIGENVECTOR COMPATIBILITY OF ANGLE PLY DEFORMATIONS

This theory section sets out to use eigenvectors of lamina stiffness matrices to indicate which ply angles allow for compatible modes of deformation in pre-cure consolidation. Square brackets, [ ] denote matrices and vectors in the text that follows.

2.1 Eigen decomposition representation of the lamina stiffness matrix

The in-plane stiffness matrix $[Q_\theta]$ of a lamina of any angle θ is always real symmetric, as such it can be subject to an eigen-decomposition;

$$[Q_\theta] = [V][D][V]^T \tag{1}$$

where $[V]$ is a matrix with normalized (unit length) eigenvectors, $[v_1]$, $[v_2]$, and $[v_3]$ of $[Q_\theta]$ as its columns (i.e. $[v_1]$, $[v_2]$, and $[v_3]$ form an orthonormal basis) and $[D]$ is a diagonal matrix with the eigenvalues, λ_{Qi} for i = 1..3, of $[Q_\theta]$ on its leading diagonal. Eigenvalues in $[D]$ are derived from solution of the classical eigenvalue problem;

$$\left[Q_\theta - \lambda_{Qi} I\right] = 0 \tag{2}$$

where [I] is the identity matrix.

Classical Lamination Theory (with the Reuter matrix $[R]$ correction for tensorial shear strain) gives the following equation for $[Q_\theta]$,

$$[Q_\theta] = [T]^{-1}[Q][R][T^{-T}][R]^{-1}$$

$$= \begin{bmatrix} c^2 & s^2 & -2cs \\ s^2 & c^2 & 2cs \\ cs & -cs & c^2 - s^2 \end{bmatrix} \begin{bmatrix} Q_{11} & Q_{12} & 0 \\ Q_{12} & Q_{22} & 0 \\ 0 & 0 & Q_{66} \end{bmatrix} \begin{bmatrix} 1 & 0 & 0 \\ 0 & 1 & 0 \\ 0 & 0 & 2 \end{bmatrix} \begin{bmatrix} c^2 & s^2 & cs \\ s^2 & c^2 & -cs \\ -2cs & 2cs & c^2 - s^2 \end{bmatrix} \begin{bmatrix} 1 & 0 & 0 \\ 0 & 1 & 0 \\ 0 & 0 & \frac{1}{2} \end{bmatrix}$$

$$= \begin{bmatrix} v_{11} & v_{21} & v_{31} \\ v_{12} & v_{22} & v_{32} \\ v_{13} & v_{23} & v_{33} \end{bmatrix} \begin{bmatrix} \lambda_{Q1} & 0 & 0 \\ 0 & \lambda_{Q2} & 0 \\ 0 & 0 & \lambda_{Q3} \end{bmatrix} \begin{bmatrix} v_{11} & v_{12} & v_{13} \\ v_{21} & v_{22} & v_{23} \\ v_{31} & v_{32} & v_{33} \end{bmatrix} \tag{3}$$

Where $[Q]$ is the stiffness matrix for a 0° ply with,

$$Q_{11} = E_{11}^2 (E_{11} - \nu_{12}^2 E_{22})^{-1}$$

$$Q_{12} = \nu_{12}E_{11}E_{22}(E_{11} - \nu_{12}{}^2E_{22})^{-1}$$

$$Q_{22} = E_{11}E_{22}(E_{11} - \nu_{12}{}^2E_{22})^{-1}$$

$$Q_{33} = G_{12}, \quad c = \cos(\theta) \text{ and } s = \sin(\theta) \tag{4}$$

E_{11} represents the Young's modulus in the fibre direction, E_{22} the Young's modulus in the resin direction and ν_{12} the major Poisson's ratio.

The diagonal matrix $[D]$ can be converted to a linear sum of three matrices each with only a single non-zero entry on the leading diagonal. Note that the structure of the three single eigenvalue matrices means that only terms from the eigenvector associated with that eigenvalue survive the matrix multiplication. It therefore is apparent that this equation can be written in an outer product form:

$$[T]^{-1}[Q][T^{-T}] = \lambda_1 \begin{bmatrix} v_{11} \\ v_{12} \\ v_{13} \end{bmatrix} [v_{11} \quad v_{12} \quad v_{13}] + \lambda_2 \begin{bmatrix} v_{21} \\ v_{22} \\ v_{23} \end{bmatrix} [v_{21} \quad v_{22} \quad v_{23}] + \lambda_3 \begin{bmatrix} v_{31} \\ v_{32} \\ v_{33} \end{bmatrix} [v_{31} \quad v_{32} \quad v_{33}] \tag{5}$$

Or in short hand,

$$[Q] = \lambda_1[v_1][v_1]^T + \lambda_2[v_2][v_2]^T + \lambda_3[v_3][v_3]^T \tag{6}$$

It should be noted that $[v_i]^T[v_j] = 0$ for i ≠ j, i.e. the dot product of any two eigenvectors for a particular ply is 0 making them orthogonal and thus the modes of deformation they represent independent. The three eigenvectors in $[v]$ for each ply are also dimensionless and normalized to have unit length. There are two choices for each eigenvector, the second of which is reached by multiplying the first by -1. However, to ensure that a physically consistent system of deformations is maintained, eigenvectors must be chosen such that the right-handed orthogonality of the three eigenvectors that represent a 0° ply is maintained for other ply orientations, i.e. after rotation, eigenvectors for plies other than 0° must maintain positive directions that are compatible with the original right-handed configuration of the eigenvectors of the 0° ply. Alternatively, the eigen-basis for a θ° ply is based on a rotation but not reflection of the 0° ply eigen-basis (non-orthogonality of the transformation matrix notwithstanding). The stiffness related to deformation in each mode is given by the associated eigenvalue in $[D]$ and thus terms in the Eqs.(5-6) have units of Pascals. Note that modes of deformation with smallest and greatest eigenvalues correspond to deformations of minimum and maximum energy respectively, i.e. modes that require soft resin deformation or stiff fibre deformation respectively. This can be seen by considering the application of Eq.(5) to the field of strain column vectors with unit length; the resulting load vector would be of minimum magnitude if the original strain vector was orthogonal to the eigenvectors associated with the two largest eigenvalues. Note that the eigenvectors for the compliance matrix, $[q]$, are identical to those of $[Q]$ but have associated eigenvalues given by the reciprocal of those of $[Q]$.

2.2 Eigen-decomposition of plies with various angles

In order to assess the formability of laminates with a given stacking sequence, it is necessary to assume that resin properties are linear elastic. Clearly, the resin is actually visco-elastic, but the results presented below provide a qualitative measure of formability. Assuming uncured material properties, E_{11} = 128 GPa, E_{22} = 0.100 MPa, G_{12} = 0.338 MPa and υ_{12} = 0.12 [6], we obtain the following eigenvectors and eigenvalues for a given uncured ply angle θ. In the results that follow, the sign convention defining tensile stress as positive and compressive stress as negative, is used to define the directions of eigenvectors $[V]$ and eigenvalues $[D]$ from a given $[Q_\theta]$. The sign convention for eigenvectors can be verified by taking the triple product, given by the product of the three eigenvectors

$[v_1]$, $[v_2]$, and $[v_3]$ for a given fibre angle. When using the correct sign convention, eigenvectors follow the right-hand rule, which is outlined by a positive scalar triple product.

	Resin Mode I				Resin Mode II				Fibre Mode			
θ	λ (kPa)	ε_x	ε_y	γ_{xy}	λ (kPa)	ε_x	ε_y	γ_{xy}	λ (kPa)	ε_x	ε_y	γ_{xy}
0	100		1		338			1	$1.28\text{x}10^8$	1		
90	100	1			338			-1	$1.28\text{x}10^8$		1	
45	67	0.41	0.41	-0.82	676	-0.71	0.71		$0.96\text{x}10^8$	0.58	0.58	0.58
-45	67	0.41	0.41	0.82	676	0.71	-0.71		$0.96\text{x}10^8$	0.58	0.58	-0.58

Table 1: Eigenvalues λ_i and eigenvectors $[v_i]$ within each deformation mode for a given ply angle θ.

Assuming that a stack of uncured plies being formed over a tool will seek to find a minimum energy deformed state, it can be hypothesized that each ply will attempt to deform in its own minimum energy (resin deformation only) state. A visual representation of single 0˚ ply deformation in all three modes is presented in Fig 1.

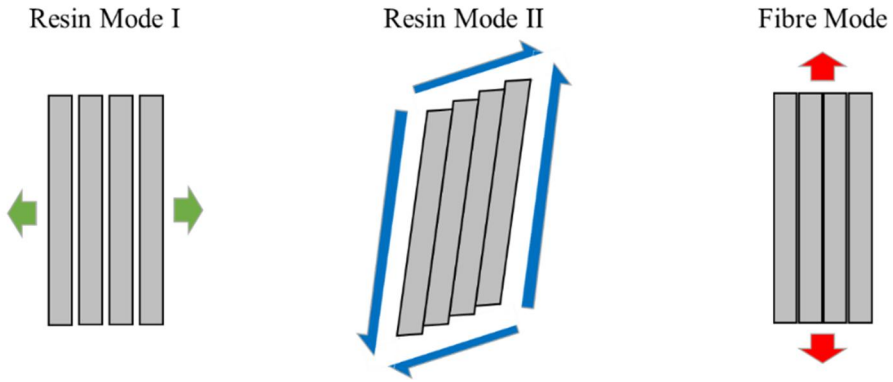

Fig 1: Distinct single ply deformation modes for 0° uncured ply

However, as can be seen from the orthogonality of eigenvectors associated with minimum eigenvalues for the 0° and 90° plies in Table 1, individual ply deformations may be incompatible and thus deformation in higher eigenvalue (higher energy) modes may be required.

For example, the eigenvectors associated with Resin Mode II in the 0° and 90° plies are identical (parallel) and thus compatible. If compatibility is not achieved for modes associated with low value eigenvalues then, as in-plane fibre deformation is energetically highly unfavourable, local out-of-plane deformation in the form of wrinkling may form part of the overall minimum energy mode for the deformed laminate (unless compatible deformations at other interfaces offset these high energy modes).

The vector dot product of two column eigenvectors in adjacent layers *k* and *k+1* given by given by

$$[v_{\propto n}]_k^T [v_{\beta m}]_{k+1} \qquad \alpha = \theta, \varphi; \quad \beta = \theta, \varphi; \quad \theta = 0{,}90; \quad \varphi = 45, -45; \quad n = 1, 2\,; \quad m = 1{,}2 \tag{7}$$

where *n* and *m* indicate eigenvectors relating to the lowest and second lowest eigenvalue respectively. Note that as the eigenvectors are normalised it holds that $-1 \leq [v_{\propto n}]_k^T [v_{\beta m}]_{k+1} \leq 1$.

An angular separation between vectors of 0 indicate parallel and thus compatible modes of deformation. Conversely, orthogonal and thus incompatible modes have a separation of 90° and thus a

dot product value of 0. Hence the vector dot product can be used to assess the compatibility of deformation of neighbouring plies. Whenever the Resin I or Resin II mode are in-line with the Fibre mode of the 2nd ply, deformation cannot happen. As a result, plies with 90° interfaces can only shear together, as both resin modes are constrained by the opposing angles fibre mode. Plies with a 0° interface are free to deform in their preferred resin mode, while 45° interfaces are forced to compromise. The most formable mode in 45° interfaces occurs when either 0 or 90 plies deform in Resin Mode II, while 45 or -45 degree plies deform in Resin mode I. Table 2 outlines the 4 possible deformation scenarios within an adjacent ply interface. A visual representation of the preferred (max value) deformation for a given fibre interface between two plies is outlined in Fig 2 below

Interface Angle	Example α/β	Deformation Mode of Adjacent Plies $[v_{\alpha1}]_1^T[v_{\beta1}]_2$	$[v_{\alpha1}]_1^T[v_{\beta2}]_2$	$[v_{\alpha2}]_1^T[v_{\beta1}]_2$	$[v_{\alpha2}]_1^T[v_{\beta2}]_2$
0°	90/90	**1**	0	0	1
45°	0/45	0.41	0.71	**-0.82**	0
45°	0/-45	0.41	-0.71	**0.82**	0
90°	0/90	0	0	0	**-1**

Table 2: Compatibility of deformation modes for a given interface

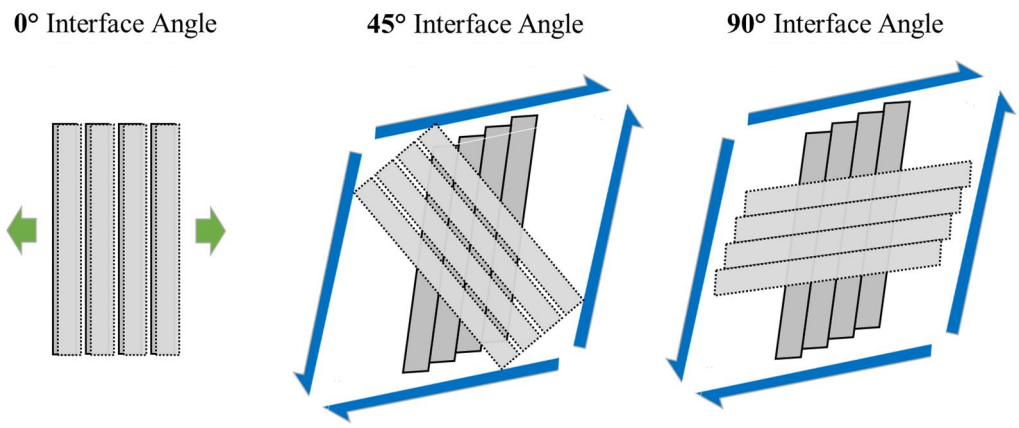

Fig 2: Chosen deformation modes of 2 plies when paired together through a given fibre interface angle

This analysis of interface angle using two adjacent plies can be extended to a full stack analysis. The interfaces continue to be treated on a simple ply-by-ply basis. In order to generate a value for multi-layer laminate compatibility, sums of vector products at each interface for a given deformation mode are taken for *N* number of plies. This is carried out for all four possible interface deformation scenarios, to determine the maximum possible laminate compatibility.

$$C_{nm} = \sum [v_{\alpha n}]_k^T [v_{\beta m}]_{k+1} + \sum [v_{\beta m}]_i^T [v_{\alpha n}]_{i+1}$$

$$k = 1,3,5,7,\dots\ N-1(\text{even } N)\ or\ N-2(\text{odd } N)$$
$$i = 2,4,6,8,\dots\ N-1(\text{odd } N)\ or\ N-2(\text{even } N)$$

$$\alpha = \theta,\varphi;\quad \beta = \theta,\varphi;\quad \theta = 0{,}90;\quad \varphi = 45,-45;\quad n = 1,2\,;\quad m = 1{,}2 \tag{8}$$

Given an example stack of 45/0/-45/90, deformation can occur in one of 4 possible scenarios. Two options require all plies to either deform purely in resin mode I or purely in resin mode II. A third possibility is presented when all θ plies deform in resin mode I, while the φ plies within the stack

deform in resin mode II. The final option would be the reverse, where θ plies act in resin mode II and φ plies in resin mode I. Carrying out this full stack interface summation for the 4 given scenarios, results in obtaining the preferred deformation state. The scenario achieving the highest C_{nm} will outline maximum stack compatibility and therefore the most formable deformation solution. When extending the multi-layer arrangements, caution needs to be taken with 45° interfaces. When a ply is met with two 45° interfaces of opposite direction, a locking behaviour occurs. Ply lockup can be detected when the compatibility value transitions from positive to negative or vice versa between two interfaces, e.g. 45/0/-45 ply sequence. This can be seen from Table 2 where the most compatible modes of 0/45 and 0/-45 outline the same magnitude of 0.82, but with different signs. In the full laminate compatibility analysis these values cancel each other out, thereby indicating locking and a resulting incompatibility. A visual representation of the ply locking behaviour is given in Fig 3; the central ply cannot deform in the preferred direction of one of the 45° plies without forcing a high energy deformation in the other 45° ply.

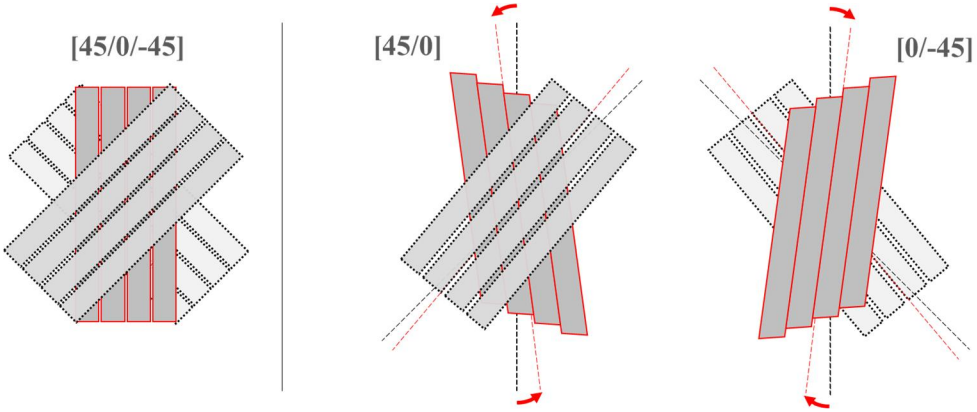

Fig 3: Three ply lock up scenario when first and third ply are at an opposing 45˚ interface to the middle ply.

This theoretical model will be used to predict the formability of a full stack, with respect to the interface angle and the positioning of plies within the stack.

3 EXPERIMENTAL METHODOLOGY

An industrial Double Diaphragm Former (DDF) provided the experimental basis for the automated forming process. The DDF raises the temperature of the laminate using heating bulbs, and creates a vacuum between the inner bag and forming bed to allow the outside atmospheric pressure to form the laminate around the given tool geometry. A sketch of the experimental set-up is shown in Fig 4. As the heating bulbs only provide heat from the top, having a temperature differential of up to 10°C within the stack, is not uncommon. Heater mats were therefore added to the inside of the tool, allowing for a consistent and uniform temperature distribution throughout the entire stack.

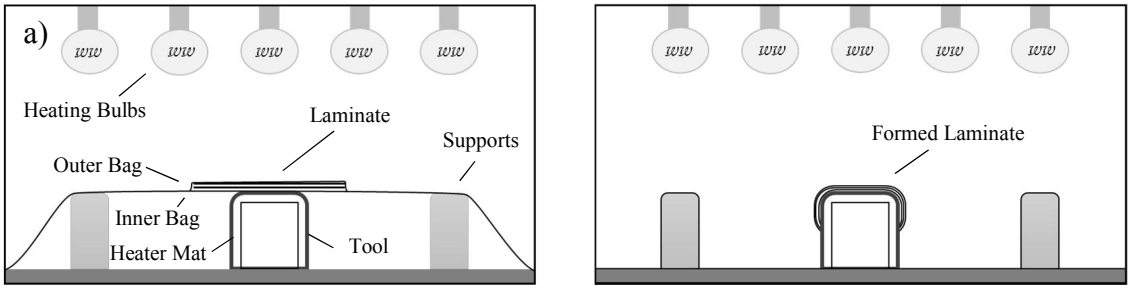

Fig 4: Forming Setup within the DDF. a) Pre-Forming. B) Post-Forming

Forming trials were conducted using 24 ply thick laminates, made of AS4/8552 UD prepreg material. Three Quasi-Isotropic (QI) layups with differing stacking sequences were investigated, as listed in Table 3. Each chosen stacking sequence outlines a system of distinct fibre interface angles, expected to show differential forming behaviour.

Sample ID	Layup	Predominant Fibre Interface Angle
QI_1	$[(\pm45)_3(0/90)_3]s$	90°
QI_2	$[(45/0/-45/90)_3]s$	45° (cont. spiralling)
QI_3	$[(45/0)_3(90/-45)_3]s$	45° (block alternating)

Table 3 Investigated 24 ply QI laminates with varying stacking sequences. Note that 0° fibres are defined along the tool length.

The experimental procedure comprised covering the flat 24 ply thick laminate with release film to create a separation layer between the prepreg material and the vacuum bag. The laminate underwent a continuous debulking cycle after being placed between the inner and outer bag, prior to evenly heating up to the desired temperature by the DDF and heater mats. Once the set temperature was reached in the laminate, draw of 0.7 bar/min until full vacuum was reached allowed the bags to stretch while conforming the laminate to the tool geometry. The formed laminate was allowed to cool while maintaining full vacuum until the stack reached a temperature below 30°C. Finally, the bags were cut to facilitate the removal of the tool and formed laminate.

Due to the size of the available industrial DDF, it was decided to manufacture a single tool that would allow for two forming operations at the same time. This would provide a higher experimental efficiency, while ensuring that forming parameters of temperature and pressure were identical for every laminate pair that was formed.

The tool was designed to create a complex part geometry that would allow for sufficient defect generation. A CFRP tool material was used due to its low CTE and high rigidity at elevated curing temperatures. The male CFRP tool was moulded from a tooling block female pattern. The geometry was inspired by Hallander's proven tool design [5], but rather than having a single recess feature on one flange, the recess was carried around the web and onto the other flange side, thereby creating a ramped spar geometry. This makes the laminate more prone to defect generation, as the material is forced to undergo larger deformations during forming. The tool design is presented below in Fig 5.

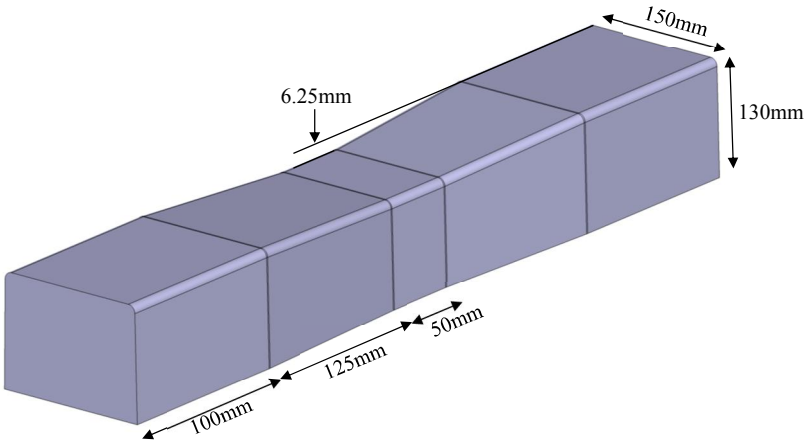

Fig 5: Tool geometry with a symmetric 1:20 ramp on both flanges and web face. The maximum and minimum Gaussian curvatures are given as $0.0127mm^{-2}$ and $-0.0155mm^{-2}$.

The formed laminates were analysed both after DDF forming and after the final cure. A Coordinate Measuring Machine (CMM) was used to measure the thickness distribution throughout the entire laminate demonstrator. This allowed for detailed formability comparison between stacks of different stacking sequences and forming parameters.

3 RESULTS

3.1 Theoretical Results

The vector dot product analysis defined in section 2 can be extended to a full laminate compatibility analysis on an interface-by-interface basis. Fig 6 indicates the compatibility of the four possible modes at every ply interface within the stacking sequences, as defined in Table 3. Assumed material properties are as given in section 2. The total laminate compatibility, as shown in Fig 7, is given through summation of the previously determined individual interface compatibilities for the most formable deformation case.

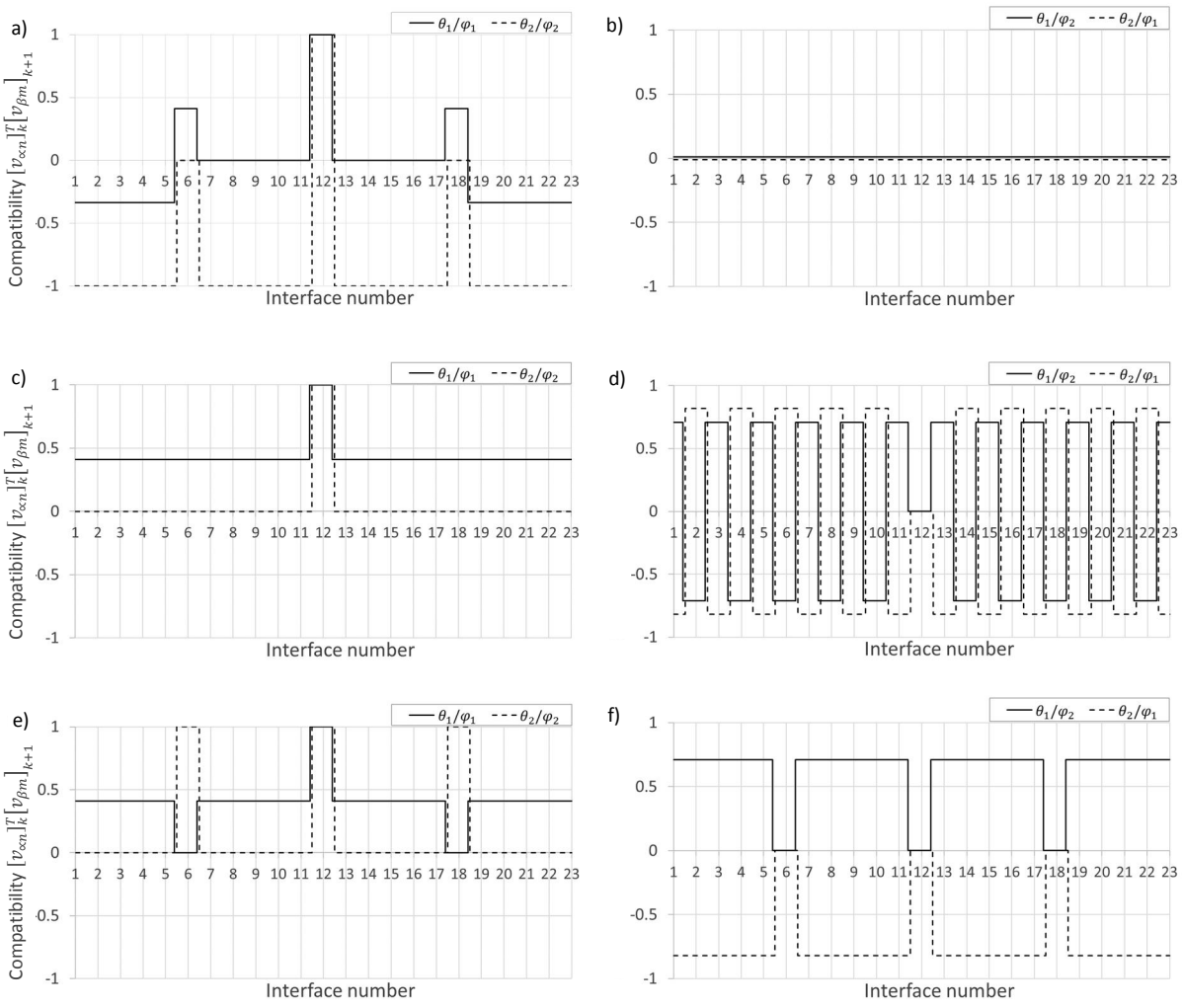

Fig 6: Interface compatibility of all four deformation scenarios throughout the entire stack for given laminates QI_1: (a) and (b); QI_2: (c) and (d) and QI_3: (e) and (f)

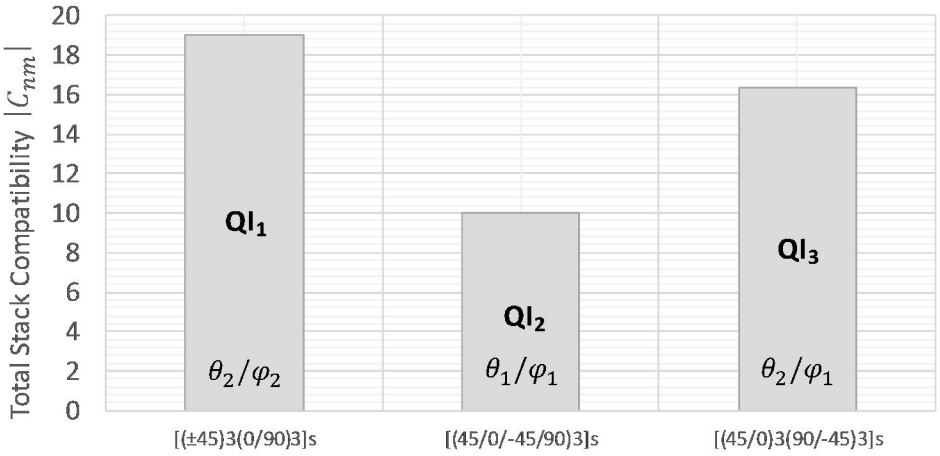

Fig 7: Total combined ply compatibility of the given laminate stack. High values predict improved laminate formability.

3.2 Experimental Results

An outline of the DDF formed laminates is presented below. Laminates undergo further consolidation after the forming process as part of the curing procedure, which is presented in Fig 8, using the example of the QI_2 laminate.

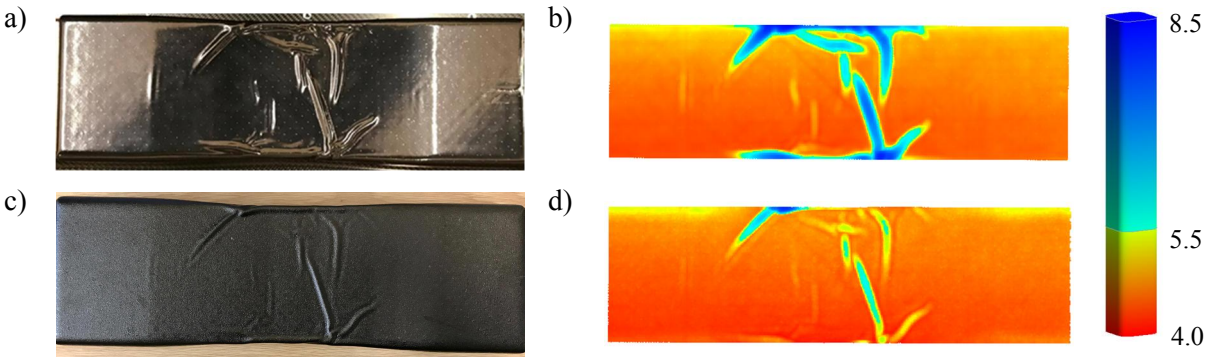

Fig 8: Forming results of QI_2 at 40ºC. a) post forming, b) post forming laminate thickness variation, c) post cure, d) post cure laminate thickness variation. Thickness variations are given in mm.

Wrinkles that have generated as a result of the forming operation, which was carried out at 40ºC, can be seen in Fig 9. The three given stacking sequences clearly outline differential forming behaviour, despite being formed under identical conditions.

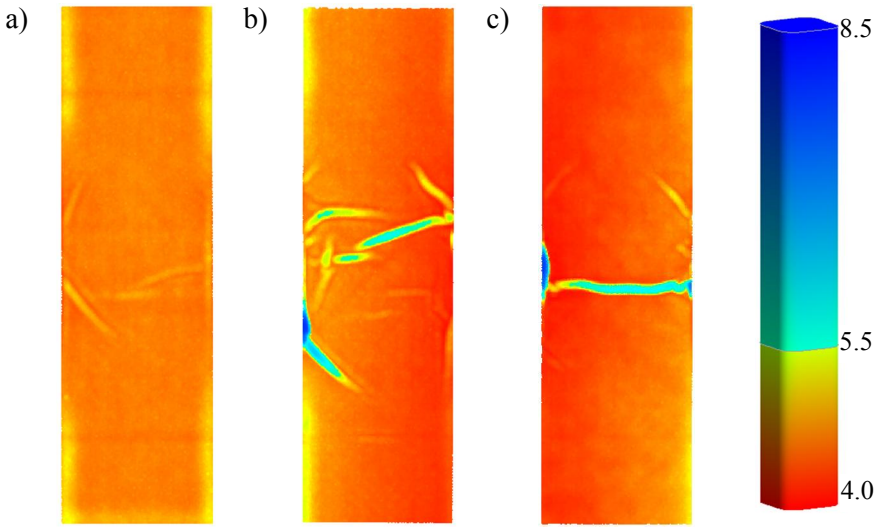

Fig 9: Thickness variations post cure for laminates (a) QI_1, (b) QI_2 and (c) QI_3. All three laminates have been formed at 40ºC. Thickness variations are given in mm.

The effect of elevated temperature during forming on the most formable and least formable laminate can be seen below in Fig 10. Despite an optimal forming temperature of 80º C, the spiralling 45º interface laminate still outlines a defect. On the other hand the formable 90º interface stack demonstrates fully defect free forming at already 60ºC.

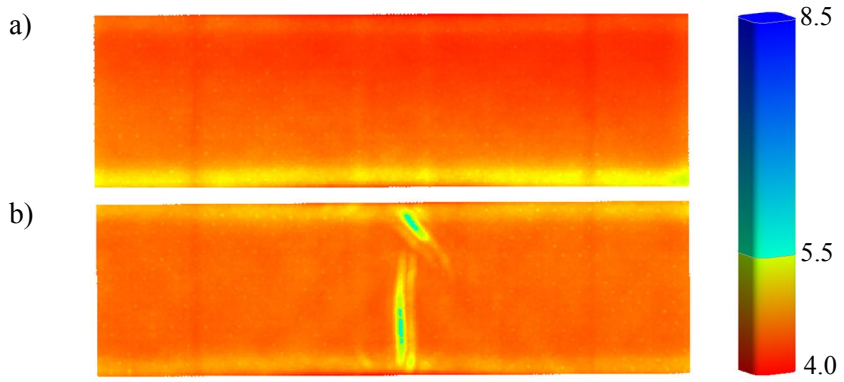

Fig 10: Laminate forming results of cured samples that have been formed at elevated temperatures for (a) QI_1 at 60ºC and QI_2 at 80ºC.

4 DISCUSSION

From Fig 6, the 24 ply QI_1 laminate with 0,90,45 and -45 plies predominantly arranged with a 90° interface angle show the highest compatibility mode of 1.0 when adjacent plies deform in resin mode II, which correlates to plies shearing together. The only disruption to this pattern appears at intersections where 0/90 arrangements meet 45/-45 ply blocks. In this case e.g. at interfaces 6 and 18, compatibility drops from full to zero compatibility. Slip planes are believed to form in those incompatible interfaces where a formable block of 0/90 is met with another formable block of 45/-45 plies. The other three deformation scenarios for QI_1 outline either complete incompatibility or a negligible amount of compatibility,. For stack QI_2 which has spiraling 45° interfaces, all plies are prevented from forming in their individually most compatible mode, as shown by the alternating nature of the compatibility plot in Fig 6 (d). Plies are therefore required to deform in a different mode. This is given where adjacent plies both deform in resin mode I, albeit at a much lower compatibility of 0.41. The third given stacking sequence QI_3 also predominantly comprises 45° ply interfaces, as with

the QI_2 stack, but significantly separates ply groups, thereby avoiding the spiraling behaviour of QI_2. As a result the laminate is not locked and therefore individual plies are free to deform in their most compatible mode, given where 0's and 90's deform in resin mode II, and 45's and -45's in resin mode I to give an individual compatibility of 0.82. Taking sums of the individual ply compatibilities within a stack provides the total stack compatibility as outlined in Fig 7. QI_1 shows the highest stack compatibility index of 19, for all 24plies. Compared to QI_1, QI_2 outlines a 47.3% reduced total stack compatibility, as expected from the spiraling 45° interfaces. The final stack QI_3 performs significantly better than QI_2, but still shows a 13.7% lower total stack compatibility compared to QI_1. Theoretically QI_1 with 90° interfaces therefore presents the most formable solution for a 24 ply stack of UD prepreg in a quasi-isotropic arrangement. When evaluating the total compatibility index C_{nm} in vector form as opposed to a dot product addition of each interface, a prediction on directionality of stack deformation can be made. QI_1 outlines a vector of [-5,-5,-9], showing that part of the plies within the stack shear in *xy*, while others stretch or compress in *x* and *y*. This behaviour however is not present in the other two laminates. QI_2 has vector [4.92,5.1,0] and QI_3 [0,0,-16.4]; both outline isolated deformations through either purely shearing in *xy*, or simply stretching and compressing in *x* and *y* directions. The lack of shear deformation in addition to the low total compatibility C_{nm} for the QI_2 combine to produce a laminate with very problematic forming behavior in comparison to the QI_1 laminate.

The experimental results as demonstrated in Fig 9 reflect what has been suggested by the theory. While all three samples where formed under identical conditions at 40°C, QI_2 clearly represents the most defective sample. The defects are not only widely spread on the web face of the part but also carry over the flange region of the part. Despite defects being present in both QI_1 and QI_3 web areas, they appear a lot less severe and fewer in number. The flange areas in both cases also outline no visible defect wrinkle. When comparing both QI_1 and QI_3, a slightly higher wrinkle severity does show up in QI_3. Elevating the forming temperature to 80°C for the least formable laminate QI_2 still does not produce a defect free part, due to the remaining wrinkle defect. However, the most formable laminate QI_1 already outlines a perfectly defect free part at only 60°C.

The correlation between the predicted theoretical formability for all three given stacking sequences and the experimentally formed samples equates to a high level of accuracy. The presented theoretical model therefore provides a simplistic and quick, but powerful tool to verify the formability of individual plies and chosen full stacking sequences.

5 CONCLUSION

The conducted research has demonstrated that the ply interface angle is a significant contributor to the formability of multi-layer composite laminates. For automated forming applications, stacking sequence should therefore be considered together with vacuum application rate and temperature, to produce the best possible result. The experimental results have shown that 90° ply interface within a stack produces the most favourable forming results. In contrast, spiralling 45° interfaces outline the lowest compatibility due to the resulting locking behaviour and therefore are most prone to defect generation, especially on doubly curved tool geometries. The experimental test program was accompanied by a successful theoretical model which predicted the experimental outcome, while taking the entire stacking sequence into account. The presented results on interface angle and the corresponding ease of manufacture does not only apply to forming procedures, but should also hold true for simple debulking conditions, such as found during an autoclave cycle.

ACKNOWLEDGEMENTS

The authors thank GKN Aerospace and especially Tony Lloyd for the technical support during the design and manufacture of the tool, the forming trials and the supply of AS4/8552 material. We also thank Dr. Andrew Francis (GKN Aerospace) for the technical assistance with writing the CMM code. Richard Butler holds a Royal Academy of Engineering/GKN Aerospace Research Chair in Composite Analysis.

REFERENCES

[1] Dodwell, T. J., Butler, R., Hunt, G. W., (2013) "A semi-analytical model for the wrinkling of laminates during consolidation over a corner radius" University of Bath

[2] Bloom, L.D., et al. (2013) "Damage progression and defect sensitivity: An experimental study of representative wrinkles in tension." Composites Part B: Engineering 45(1): 449-458

[3] Sun, J., et al. (2012). "Effect of forming temperature on the quality of hot diaphragm formed C-shaped thermosetting composite laminates." Journal of Reinforced Plastics and Composites 31(16): 1074-1087.

[4] Wei-Ting Wang, H. Y., Kevin Potter and Chul Kim (2016). Improvement of composite drape forming quality by enhancing interply slip. ECCM17. Munich, Germany

[5] Hallander, P., Akermo, M., Mattei, C., Petersson, M., Nyman, T., (2013) "An experimental study of mechanisms behind wrinkle development during forming of composite laminates" Composites: Part A 50 54-64

[6] M.W.D. Nielsen, K. Johnson, A.T. Rhead and R. Butler, Laminate design for optimized in-plane performance and ease of manufacture, ICCM21 – 21st International Conference on Composite Materials, Xi'an, China, 20-25th August 2017